THE JOURNAL OF PHYSICAL CHEMISTRY B
A JOURNAL OF THE AMERICAN CHEMICAL SOCIETY

pubs.acs.org/JPCB

Article

Temperature-Dependent Conformational Evolution of SARS CoV-2 RNA Genome Using Network Analysis

Published as part of The Journal of Physical Chemistry virtual special issue "Kankan Bhattacharyya Festschrift".

Omkar Singh, Pushyaraga P. Venugopal, Apoorva Mathur, and Debashree Chakraborty*

Cite This: *J. Phys. Chem. B* 2021, 125, 10672–10681

Read Online

ACCESS | Metrics & More | Article Recommendations | Supporting Information

ABSTRACT: Understanding the dynamics of the SARS CoV-2 RNA genome and its dependence on temperature is necessary to fight the current COVID-19 crisis. Computationally, the handling of large data is a major challenge in the elucidation of the structures of RNA. This work presents network analysis as an important tool to see the conformational evolution and the most dominant structures of the RNA genome at six different temperatures. It effectively distinguished different communities of RNA having structural variation. It is found that at higher temperatures (348 K and above), 80% of the RNA structure is destroyed in both the SPC/E and mTIP3P water models. The thermal denaturation free energy change $\Delta\Delta G$ value calculated for the long-lived structure at higher temperatures of 348 and 363 K ranges from 2.58 to 2.78 kcal/mol for the SPC/E water model, which agrees well with the experimentally reported thermal denaturation free energy range of 2.874 kcal/mol of SARS CoV-NP at normal pH. At higher temperatures, the stability of RNA conformation is found to be due to the existence of non-native base pairs in the SPC/E water model.

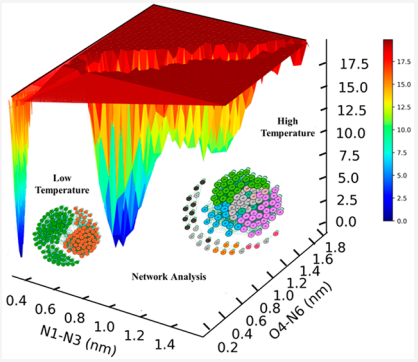

1. INTRODUCTION

The potential of pathogenic RNA viruses to adapt to various environmental factors poses a great threat for disease control and management. Current limitations in the experimental procedures to understand the RNA structure–dynamics–function relationship affects the process of vaccine and drug discovery which targets viral RNA genome.[1] This creates the need for theoretical investigation of the structure–function relation of this macromolecule. The frameshift stimulation element (FSE) from SARS CoV-2 RNA genome is an ideal drug target for designing and developing antiviral drugs against the COVID-19 pandemic. The biological functions of this RNA element are related to 3-stem pseudoknot structures, which regulate the expression of essential viral proteins. Experimental reports suggest that the rapid spread of SARS CoV-2 is generally due to low temperature and relative humidity.[2]

Study of the folding–unfolding–misfolding mechanism and energy landscape of biomolecules gives meaningful information regarding the microstates of the system which govern its stabilization and biological functions. However, several challenges stand in the way of using energy landscapes of macromolecular systems like RNA to relate with the structure and dynamics to function. One big problem in handling such a big system is the handling of the data. Because of this drawback, coarse-graining of the biomolecules is becoming more popular at the expense of the atomistic detail of the simulations. On the other hand, atomistic molecular dynamic simulation can give us proper detail regarding a process, but computation of the long trajectories of macromolecular systems is computationally prohibitive. In addition, long and multiple simulations are required to ensure proper sampling of the data. One very important characteristic of proper sampling of the data is we should not miss any important information presented happening during the process of the evolution of the trajectories; at the same time we cannot focus on very minute details of such big systems because that will create unnecessarily large data which are of insignificant use. In this article, we introduce a network analysis method that can sample big data sets effectively to identify the most prominent conformations of the macromolecules like RNA, which existed during the process of evolution/denaturation and can also show how these conformations are connected to each other. Network analysis has been successfully used in other disciplines such as social and behavioral sciences[3] but has not been applied in RNA systems. This method can depict meaningful information such as the prominent conformations of the RNA, which otherwise is averaged out statistically. The

Received: June 30, 2021
Published: September 15, 2021

https://doi.org/10.1021/acs.jpcb.1c05795
J. Phys. Chem. B 2021, 125, 10672–10681

beauty of this process is that a particular conformation of RNA can be represented as a node. The similarity or disparity between the conformations can be determined by fixing some energy-based or geometry-based criteria. If the conformation changes, it is denoted by another node. An edge denotes the evolution of one conformation to another conformation. This helps us to show the structural evolution of the RNA molecule in a simplified way with a decreased amount of handling of data and complexities. It also helps to locate the conformation of the RNA which existed for the maximum time throughout the trajectory and the most well-connected conformations. Network analysis links the data quickly and effectively without leaving out important information about the system, and therefore, it helps in the effective understanding of the structure−function relationship. For a detailed analysis, we compared the results of RNA simulations using two water models: SPC/E model and modified TIP3P model. The system and computational details are given in Materials and Methods. The results and the possible explanations are given in Results and Discussion. The major outcomes are provided in Conclusion.

2. MATERIALS AND METHODS

2.1. Molecular Dynamics Simulation. SARS CoV-2 RNA FSE (PDB ID: 6XRZ[4]) was simulated by GROMACS[5] using CHARMM force field.[6] It is believed that FSE contains a major ring binding site and other two alternative binding sites: slippery hairpin site and J3/2 site, where small molecules can bind to perform antiframeshifting.[4] The frameshifting process helps the virus to compact larger genetic material into short genetic elements.[7,8] Small drug molecules which bind to the FSE binding site can cause antiframeshifting, which blocks the production of RNA enzymes important for viral replication.[9] The binding of the drug molecules depends on the conformation of the pseudoknot structure in SARS coronavirus,[10] which is identical to SARS CoV-2 FSE up to single-nucleotide substitution.[4] Therefore, studying the conformation evolution of FSE from SARS CoV-2 RNA genome with temperature change can help to understand the finer details of the major forces responsible for maintaining the biological activity of RNA. Two independent sets of 250 ns simulations (total 12 simulations) were performed to study the structural and dynamic behavior of the RNA genome at six temperatures: 288, 303, 318, 333, 348, and 363 K (Table S1) using the SPC/E water model.[11] This temperature range is selected because the thermal denaturation of SARS-CoV was reported at a temperature range of 56−75 °C, experimentally.[12] The RNA molecule was solvated in a periodic cubic box with a distance of 9 Å from the box boundary. The charge of the system is neutralized by adding Na^+ ions. The energy minimization was done by steepest descent algorithm with a maximum of 50 000 steps. LINCS constraints[13] were used to restrain the bond involving hydrogen atoms. A 10 ns *NVT* equilibration was carried out using a *V*-rescale temperature coupling method[14] with a time step of 2 fs. Next, a 10 ns *NPT* equilibration was carried out with a time step of 2 fs at 1 atm using a Nosé−Hoover thermostat[15] and Parrinello−Rahman pressure coupling scheme,[16] respectively. The long-range electrostatic interactions were calculated by particle mesh Ewald method[17] and Fourier spacing of 0.16 nm. The short-range van der Waals cutoff was fixed to 1.2 nm. Finally, a 250 ns *NPT* production run was performed until the RMSD converged for all the systems. Individual atomistic molecular dynamics (MD) simulations are effective for larger systems like the RNA genome than temperature replica−exchange molecular dynamics (T-REMD) simulations. T-REMD cannot enhance sampling effectively for larger systems as the number of replicas needed to bridge the temperature is prohibitive and the increase in temperature does not provide the proper conformational transition.[18] The simulations were replicated twice to check the reproducibility of the results. Further, a set of simulations (6 simulations) were performed using a modified TIP3P (mTIP3P) water model[19] to determine the stability and structural evolution of RNA at 6 different temperatures, and the results are provided in the Supporting Information.

2.2. Network Analysis. The conformations for network analysis were obtained by an in-built clustering algorithm in GROMACS software using RMSD as the criterion. A cutoff value of 1.5 Å RMSD was selected to distinguish between 11 500 structures extracted from the 250 ns trajectory saved at a time interval of 0.02 ns for each temperature. The selection of a proper cutoff is crucial because a lower cut off value gives too many conformations, which may lead to irrelevant results, whereas a larger cutoff value neglects the finer details of the conformations. The total number of conformations increases because of the random motion of the atoms with the rise in temperature (Figure 1).

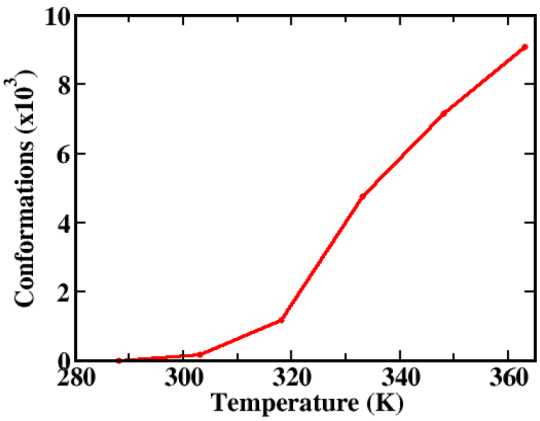

Figure 1. Distribution of the number of conformations with temperature.

In this process, we observed the presence of conformations that existed for smaller time scales and also for longer time scales. To ensure the selection of diverse conformations for the calculations, most prominent conformations from each temperature were identified based on the frequency of its existence in the whole trajectory, and network analysis was performed. We considered conformations which existed for ≥120 ps to determine the interconnectivity between the conformations. Two conformations are considered to be connected if $d(t, t') < 7.5$ Å, which is calculated by the following equation:

$$d(t, t') = \sqrt{\frac{1}{N}\sum_{i=1}^{N}(\delta_i(t))^2} \quad (1)$$

where δ_i is the distance between atom i at time t' with the reference conformation of N number of heavy atoms at time t. This criterion was chosen because the PDB ID taken has resolution around 6.9 Å. Therefore, it is better not to choose

https://doi.org/10.1021/acs.jpcb.1c05795
J. Phys. Chem. B 2021, 125, 10672−10681

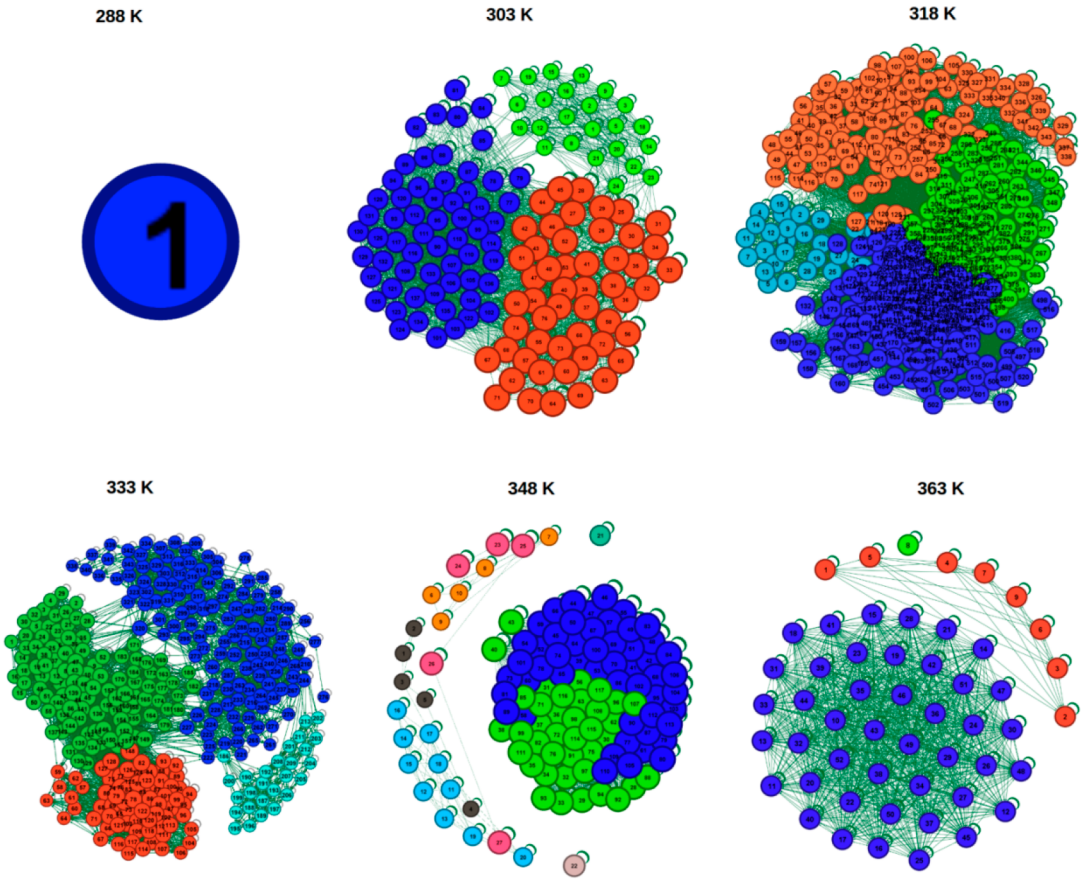

Figure 2. Network distributions of most prominent conformations at different temperatures.

the cutoff value much less than 6.9 Å. We carried out network analysis for both $d(t, t') < 7.5$ Å and < 6.5 Å. Change in the $d(t, t')$ value to 6.5 Å did not change the trend of the analysis (Figure S1). Therefore, we fixed $d(t, t') < 7.5$ Å. Selecting a much higher cutoff value reduces the number of different conformations and masking of finer detail information.

In the network map, each different conformation is represented by a node (circles) and the connectivity between the nodes is represented by the edges (lines). If two conformations are found to be connected, they are represented by two circles connected by a line. At high temperatures, there is every possibility that the conformation of the RNA can revert back to its initial configuration from where it evolved because the barrier height is easy to cross over. Therefore, each conformation of the trajectory considered was matched with all other conformations to draw the connectivity of the network map. The node and edge list were made by using eq 1, and the network distribution of the conformations was plotted using visualization software Gephi 0.9.2. The layout of the networks is determined using the Fruchterman−Reingold layout, a force-directed layout algorithm in which the edges move closer or far apart, minimizing the equilibrium energy.[20] The size of the nodes is proportional to the number of the connectivity. More connected nodes are bigger in size. The distribution of the nodes and edges give rise to different communities. Nodes with similar conformations belong to the same communities. We will discuss this in detail in Results and Discussion.

3. RESULTS AND DISCUSSION

The structural analyses (RMSD and rGyr) of the macromolecules often show misleading information about the temperature-dependent stability of RNA and its evolution (Figure S2), which shows the need for more reliable structural parameters and sampling technique to define the stability aspect. In this respect, the network analysis is performed. The representations plotted by Gephi are shown in Figure 2, which give us the information about the evolution of the structures and their connectivity. Different colors represent different communities. At lower temperature, 288 K shows only one community, which indicates that the conformation of the RNA molecule has not changed considerably in contrast to the higher temperatures. With rise in temperature up to 348 K, there is an increase in the number of communities, suggesting different conformations. The free energy of the highest connected conformation corresponding to a particular community is given in Table 1 and is calculated as follows:

$$\Delta G = -k_B T \ln(P_{rmsd}) \quad (2)$$

where P_{rmsd} is the probability distribution.[21]

The separation between the communities gives information about the different conformations. These conformations are structurally different and can have the same or different energies. For instance, the cyan and blue communities at 318 K have similar ΔG values, meaning two very different conformations have similar energies. If a community is densely populated and well-connected, it shows that the conformation existing there is stable and will have lower energy. Scarcely

https://doi.org/10.1021/acs.jpcb.1c05795
J. Phys. Chem. B 2021, 125, 10672−10681

Table 1. Network Analysis of Conformations with Respect to Temperature

	SPC/E model	
temperature (K)	conformation ID	energy (kcal/mol)
288	1 (blue)	−1.71
303	24 (green)	1.22
	47 (orange)	−2.45
	114 (blue)	−2.43
318	179 (cyan)	−3.72
	184 (blue)	−3.70
	230 (orange)	−1.08
	243 (green)	−3.30
333	128 (orange)	−2.12
	133 (green)	−2.84
	207 (cyan)	−0.61
	247 (blue)	−2.63
348	3 (brown)	−0.78
	10 (orange)	3.26
	18 (cyan)	−1.47
	26 (pink)	−0.78
	56 (green)	−1.01
	86 (blue)	−1.13
363	2 (orange)	9.94
	8 (green)	3.62
	43 (blue)	−2.37

populated and scattered communities at 348 and 363 K (for example, orange) have higher ΔG values, showing unstable conformations. Two overlapping communities can have similar ΔG values, as seen at 318 and 348 K for cyan-blue-green and blue-green communities, respectively. At 348 and 363 K, there is a clear separation between the outer ring communities and inner ring communities. This suggests that there is a considerable change in the conformation of RNA at higher temperature, which is very much different from the initial reference structure. The RNA has formed some stable structures which cannot revert to the initial structures. The blue community in this temperature is found to be stable during the simulation.

The RNA structural variation in each community with respect to temperature can be distinguished by base pair twist and width of minor−major grooves. The common RNA A-form helix is characterized by a narrow major groove and a wider minor groove.[22] The groove widths are measured from phosphate to phosphate, including the diameter of phosphate groups.[23] It is evident from Figure 3 that the representative conformations from each community are structurally different based on base pair groove width. It is found that the number of identified base pairs varies within the communities for each temperature. At 303 K, the three communities identified have different structures based on the groove width. At 318 and 333 K, the cyan community has a different structure while orange-green-blue communities have overlapping base pairs with variation in minor−major grooves. It can be seen that the major groove for 318 K is wider than that for 333 K, indicating a structural change from common RNA A-form helix. For higher temperatures, 348 and 363 K, the outer and inner ring communities have different minor and major groove positions, indicating a structural evolution. This is further supported by the twist angle, which measures the rotation of base pairs along the helical axis. The base pair twist angles are calculated and averaged with error based on the presence of minor−major grooves in the RNA structure. The standard twist angle for A-form of RNA is 32° ± 8° which is retained in lower temperatures, 288 and 303 K. At higher temperatures, the twist angle is either more twisted or less twisted for the communities with large deviations in the values, suggesting the evolution of conformations different from the A-form (Figure S3). The scatter plots show that the network distribution has effectively distinguished the communities having structural variation.

For the mTIP3P water model, we observed an increase in the number of conformations with increase in the temperature up to 348 K. At 363 K, there is a decrease in the number of conformations. The conformation of the RNA was found to disrupt completely in this temperature, and not much change in the structure was observed. The network distribution for the mTIP3P water model is shown in Figure S6. Overall, there is an increase in the number of conformations in each community compared to the SPC/E model. The conformations from each community have different structures based on twist angle and minor−major groove distance, as evident from Table S2. In the mTIP3P model, it is observed that the denaturation process of the RNA structure initiated from lower temperature (as low as 303 K). At almost every temperature we found the structure is denatured (the helix structure is destroyed) at longer simulation run, which is evident from the major−minor groove distance. Experimentally, it is found that SARS coronavirus gets denatured and converted to be noninfectious above 330 K.[24] Even though SARS CoV-2 is genetically distant from SARS coronavirus, SARS CoV-2 shares 79% genomic identity with SARS CoV.[25] Therefore, we focused our calculations mainly with the SPC/E model in the following sections. The difference in the RNA structure is noticed because of the presence of different parameters in the SPC/E and mTIP3P water models.

Next we were interested to see the fluctuations in the RNA structures which lead to these conformational changes.[26] In Figure 4, we have shown the degree of magnitude and direction of the fluctuations in RNA by porcupine plots with respect to atom C1′. The highlighted base pairs represent the variation of the native closed base pair distribution in the final conformation of RNA with temperature. Any change in the color of the base pairs with respect to the 288 K structure is due to change in the distance between the base pairs. Lesser fluctuations and a greater number of native closed base pair at 288 and 303 K indicate that native characteristics of RNA are preserved at this temperature. At 288 K, most of the closed base pairs (80%) lie in the lower-energy region I (blue), whereas we can see the emergence of different colors with the rise of the temperature. At higher temperatures (333 K and above) the number of the closed native base pairs is found to be reduced drastically because of higher fluctuations resulting in breaking of bonds between the base pairs and opening of the stem-2 pseudoknot. The existence of the non-native base pair is seen at higher temperatures leading to partial stabilization (Figure S4). The distance criteria for closed base pairs can be further confirmed by the free energy surface plotted using N1−N3 and C1′−C1′ distances of the base pairs in RNA as the reaction coordinates (Figure 5). The native structure of RNA and the final conformations of each temperature are considered in the calculation. The minimum-energy region corresponding to the closed base pairs in RNA is divided into regions I−IV. It can be seen that at lower temperatures, 288 K (black dots) and 303 K (red dots), the base pairs lie mostly in the allowed region. At higher temperatures, such as 348 K

https://doi.org/10.1021/acs.jpcb.1c05795
J. Phys. Chem. B 2021, 125, 10672−10681

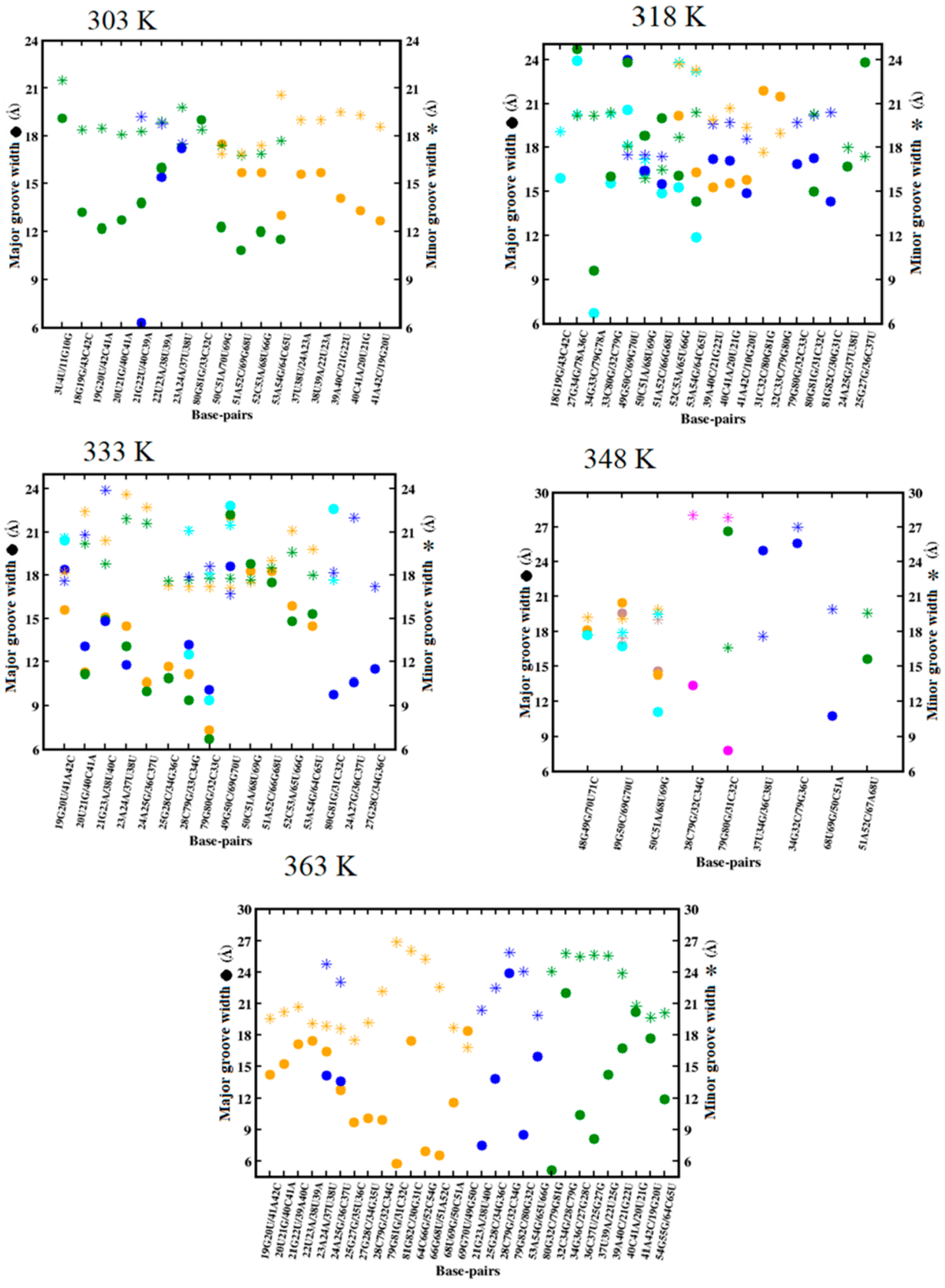

Figure 3. Scatter plot of groove width vs base pairs for 5 different temperatures in SPC/E water model.

(orange dots) and 363 K (magenta dots), the base pairs are scattered and mostly lie outside the allowed region. This shows that the characteristic distance corresponding to a closed base pair corresponds to some specific N1−N3 and C1′−C1′

https://doi.org/10.1021/acs.jpcb.1c05795
J. Phys. Chem. B 2021, 125, 10672−10681

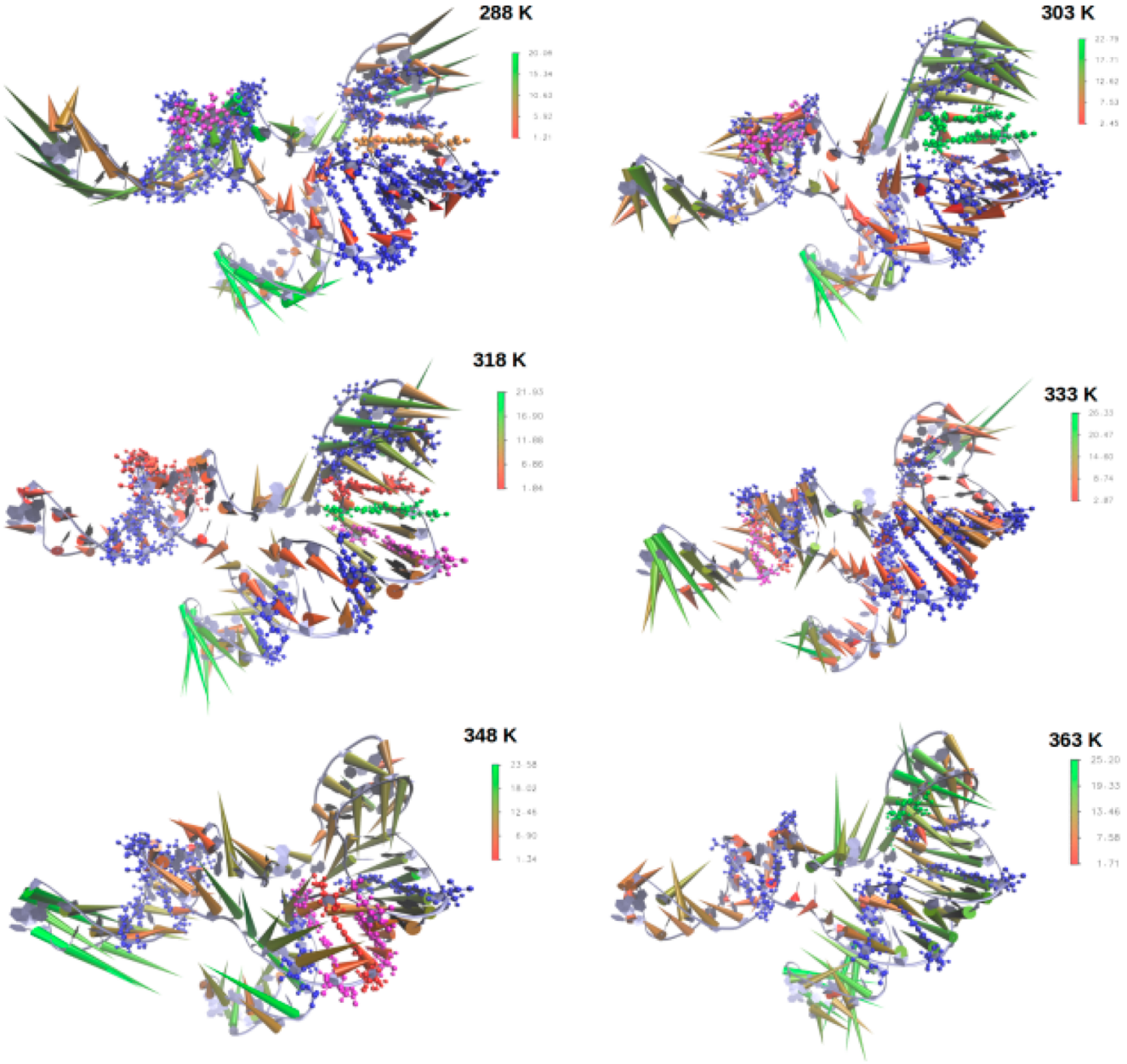

Figure 4. Porcupine plot showing the degree of fluctuation during the course of simulation

distance range irrespective of temperature. However, the open base pair can have any distance range outside the allowed region.

The percentages of native base-pair opening/denaturation of RNA for the SPC/E model at 333, 348, and 363 K are found to be 65%, 80%, and 80%, respectively, whereas in the mTIP3P model at these temperatures are 85%, 90%, and 95%, respectively. Experimentally, it is found that SARS coronavirus gets denatured at above 338 K.[24] It can be seen that the process of denaturation is higher in the mTIP3P water model. The free energy change, ΔG, can be calculated from this percentage of closed and open base pair ratio and is given by

$$\Delta G = -K_B T \ln\left(\frac{1 - f_{open}}{f_{open}}\right) \quad (3)$$

where f_{open} is the fraction of open base pairs.[27] We considered both native and combined effects of native−non-native base pairing for the comparison. Change in the temperature-induced formation of some new base pairs (non-native) is seen mainly in the SPC/E model. For native base pairs, f_{open} is the fraction of open base pairs with respect to the native structure of RNA. The free energy associated with the long-lived conformation from the network analysis for each temperature is plotted in Figure 6. The value of ΔG is found to be negative up to 318 K in the case of the SPC/E model, and it changed to a positive value at higher temperatures because of the base pair opening, which affects the stability and activity of RNA. It can be seen that consideration of the non-native closed base pairs above 318 K increases the destabilization energy at higher temperatures. In the SPC/E water model, at lower temperature (288 K), the free energy of the RNA having native and non-native base pairing is found to be −1.58 kcal/mol. The ΔG

https://doi.org/10.1021/acs.jpcb.1c05795
J. Phys. Chem. B 2021, 125, 10672−10681

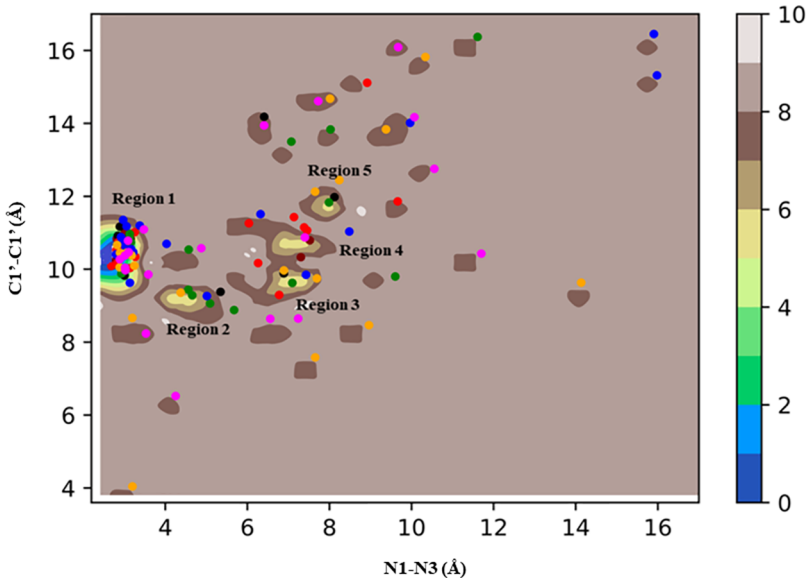

Figure 5. Free energy surface plotted using N1−N3 and C1′−C1′ distance (Å) as reaction coordinates. The blue to yellow contour regions correspond to the closed base pairs present in RNA which can be divided into regions 1−5. The base pair distances from the final structure of RNA for all the temperatures were plotted in different color dots to check the presence of native, non-native, and opened base pairs: native (maroon), 288 K (black), 303 K (red), 318 K (green), 333 K (blue), 348 K (orange), and 363 K (magenta).

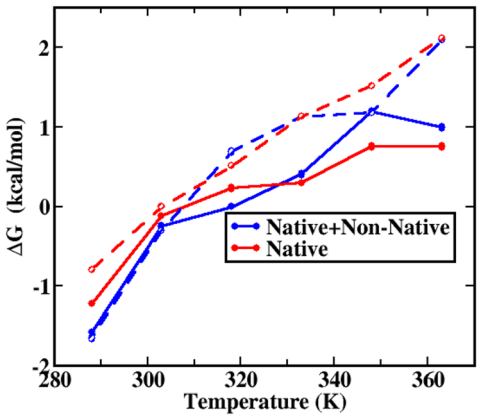

Figure 6. Free energy vs temperature. Solid and dashed lines represent ΔG values for the SPC/E and mTIP3P water models, respectively.

showed a rapid increment from 288 to 303 K for both native and non-native cases; from 303 to 318 K, the steepness of the slope decreases, showing lesser change in the ΔG value, and then there is a steep rise beyond 333 K. The $\Delta\Delta G$ value between 288 and 363 K for native and combined effect of base pairing is found to be 1.98 and 2.578 kcal/mol, respectively, which clearly shows the inactivity of RNA due to structural change in the SPC/E water model.[28,29] For 348 K, it was found to be 1.98 and 2.78 kcal/mol for native and combined effect of base pairing, respectively. The $\Delta\Delta G$ value due to structural change in the mTIP3P water model at 363 K is 2.913 and 3.743 kcal/mol for native and combined effect of native−non-native base pairing, respectively. The calculated $\Delta\Delta G$ values for the long-lived conformations agree well with the thermal denaturation free energy, 2.874 kcal/mol, of SARS CoV-NP (isolated BJ01) at pH 7 at 315 K by fluorescent intensity emission λ_{max} and CD ellipticity at 222 nm.[30] For the SPC/E water model, the $\Delta\Delta G$ values of 303 and 318 K are found to be in the range of 0.24−0.35 kcal/mol, showing similar activity of the RNA in this temperature range; this region also corresponds to the active region of transmission of the virus. The RNA structure is found to be stable at 363 K compared to 348 K because of the non-native base pairing (blue solid line).[31] It can be noted that the ΔG values considering the native base pairing for 348 and 363 K are the same (red solid line). At this temperature, only 20% of the native conformation existed. The RNA has refolded to some other structure by forming non-native bonds mainly at 363 K, which is also seen in the network analysis. At higher temperatures, the thermal fluctuation of the atoms increases, which increases the possibility of breaking of the bonds between the native base pairs. This also increases the possibility of forming new bonds between two different bases to from non-native base pairs. However, the strength of these bonds is less than that of the native bonds. The increase in the number of base pairs at higher temperatures is mainly due to the thermal fluctuations which contract the RNA structure and decrease the R_g values (Figure S2). These conformations are however not stable as the native structure. The ΔG values are higher in the case of the mTIP3P water model, which increases with the increase in the temperature.

To see the stability of a conformation, we calculated the change in the G:C base pair distance. Because these base pairs are present throughout the RNA, any change in their base pairing distance can give us information about the stability of a conformation. We focused on the radial distribution function (RDF), $g(r)$, of three intramolecular hydrogen bonds between guanine (G) and cytosine (C), namely, $N_4H\cdots O_6$, $N_1H_1\cdots N_3$ and $N_2H\cdots O_2$. As is evident from the figures, the first peak mainly lies within 2.9 Å followed by the second peak around 3−4 Å. The presence of sharp peaks at low temperatures indicates strong hydrogen bonds between the G:C base pairs, whereas the reduced peak height at higher temperatures (348 and 363 K) indicates lesser hydrogen bond strength (Figure 7). The RDFs indicate the high stability of the G:C base pair at low temperatures as compared to high temperatures. Therefore, we defined a G:C base pair being unchanged if the

https://doi.org/10.1021/acs.jpcb.1c05795
J. Phys. Chem. B 2021, 125, 10672−10681

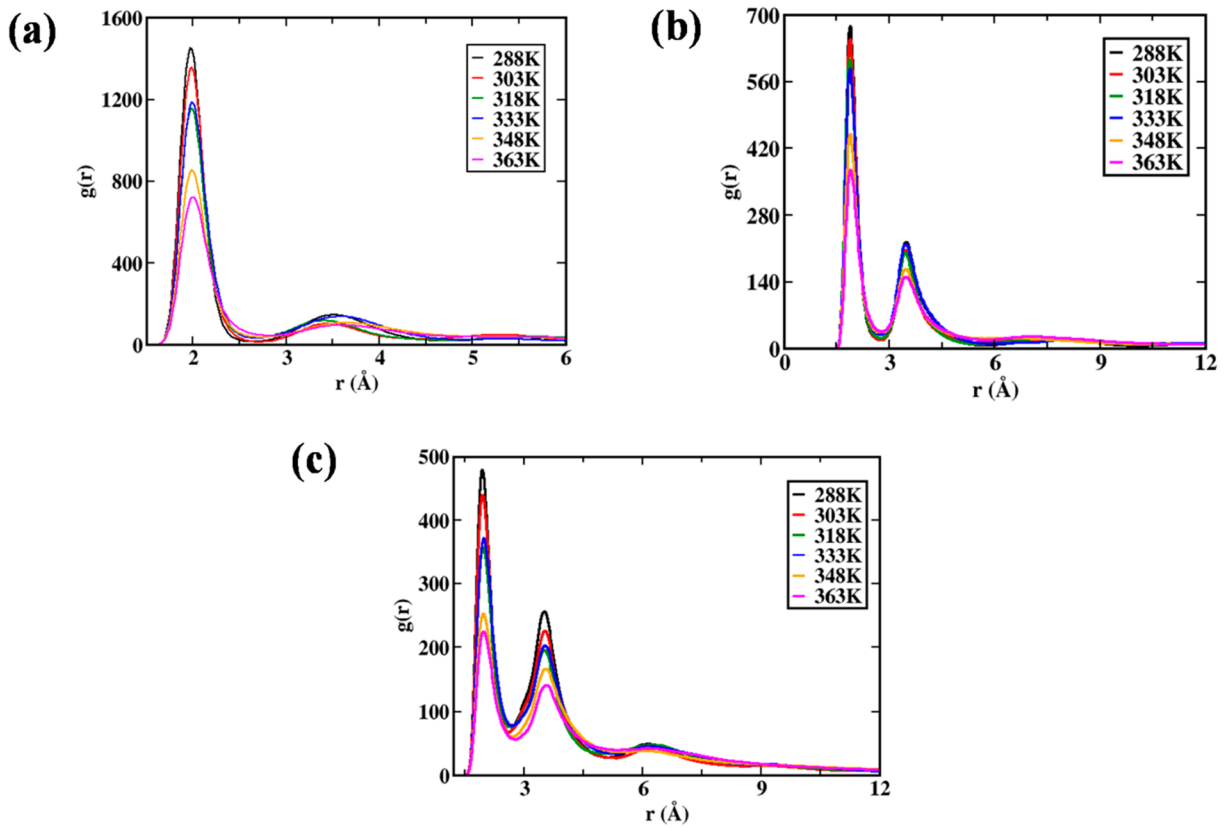

Figure 7. Radial distribution functions of different atoms of G:C base pairs with respect to temperature: (a) N−H_1, (b) O_2−H_2, and (c) O_6−H_4.

distance between any of the three hydrogen bonds present in G:C is less than or equal to 2.9 Å and changed otherwise. If this distance is continuously maintained from time $t = 0$ to t, $P(t) = 1$ and 0 otherwise.

$$S_{G:C} = \frac{\langle p(t_0) \cdot P(t) \rangle}{\langle p(t_0)^2 \rangle} \quad (4)$$

It is evident from Table 2 that as the temperature increases, the $S_{G:C}$ value decreases, indicating frequent changes of the conformations. However, it can be noticed that at 363 K, the $S_{G:C}$ value is higher than 348 K, indicating conformational stability due to the formation of non-native base pairs in the SPC/E model.

Table 2. Time Span of Conformational Evolution

	time span (ps)	
temperature (K)	SPC/E model	mTIP3P model
288	5850.30	3999.41
303	4429.83	3739.44
318	2723.55	3310.27
333	2096.19	2258.12
348	876.60	1080.78
363	1181.91	886.90

4. CONCLUSION

To conclude, we presented the conformational evolution of the SARS CoV-2 by network analysis, which gives us the information about the connectivity of the conformations and the existence of the most probable conformation of RNA at a particular temperature. The groove width and the twist based on minor−major grooves clearly show that the clustering method can efficiently distinguish the temperature-dependent conformational evolution. The ΔG value of the long-lived conformation shows stabilization of the RNA at 363 K with respect to 348 K due to formation of non-native contacts in SPC/E water model. In this model, it is seen that in the temperature range from 303 to 318 K, the ΔG values are comparable; the RNA shows similar activity in this region while at higher temperature; the structure of RNA changes a great deal because of the formation of the non-native contacts which determines its stability. The $\Delta\Delta G$ values corresponding to 80% denatured structure of RNA at 348 K and above are found to be in the range of 2.58−2.78 kcal/mol, which correlate well with experimental data. The RNA conformation in the mTIP3P water model denatures at lower temperature.

■ ASSOCIATED CONTENT

Supporting Information

The Supporting Information is available free of charge at https://pubs.acs.org/doi/10.1021/acs.jpcb.1c05795.

System details for the simulation, RMSD and rGyr profile, network distribution at a cutoff value 6.5 Å, base pair twist angle distribution, mispairing/non-native base pair information, mTIP3P water model results, and SPC/E water model second set details (PDF)

■ AUTHOR INFORMATION

Corresponding Author

Debashree Chakraborty − *Biophysical and Computational Chemistry Laboratory, Department of Chemistry, National*

https://doi.org/10.1021/acs.jpcb.1c05795
J. Phys. Chem. B 2021, 125, 10672−10681

Institute of Technology Karnataka, Mangalore, Karnataka 575025, India; orcid.org/0000-0002-0142-7941; Email: debashree@nitk.edu.in

Authors

Omkar Singh − *Biophysical and Computational Chemistry Laboratory, Department of Chemistry, National Institute of Technology Karnataka, Mangalore, Karnataka 575025, India*

Pushyaraga P. Venugopal − *Biophysical and Computational Chemistry Laboratory, Department of Chemistry, National Institute of Technology Karnataka, Mangalore, Karnataka 575025, India*

Apoorva Mathur − *Biophysical and Computational Chemistry Laboratory, Department of Chemistry, National Institute of Technology Karnataka, Mangalore, Karnataka 575025, India*

Complete contact information is available at: https://pubs.acs.org/10.1021/acs.jpcb.1c05795

Notes

The authors declare no competing financial interest.

■ ACKNOWLEDGMENTS

Funding from Science and Engineering Research Board, Department of Science and Technology, Government of India (CRG/2019/000578) is gratefully acknowledged. We thank Department of Chemistry NITK Surathkal for their constant support.

■ REFERENCES

(1) Rodrigues, J. P. G. L. M.; Barrera-Vilarmau, S.; Teixeira, J. M. C.; Sorokina, M.; Seckel, E.; Kastritis, P. L.; Levitt, M. Insights on Cross-Species Transmission of SARS-CoV-2 from Structural Modeling. *PLoS Comput. Biol.* **2020**, *16* (12), No. e1008449.

(2) Aboubakr, H. A.; Sharafeldin, T. A.; Goyal, S. M. Stability of SARS-CoV-2 and Other Coronaviruses in the Environment and on Common Touch Surfaces and the Influence of Climatic Conditions: A Review. *Transboundary Emerging Dis.* **2021**, *68*, 296.

(3) Hevey, D. Network Analysis: A Brief Overview and Tutorial. *Health Psychol. Behav. Med.* **2018**, *6* (1), 301−328.

(4) Zhang, K.; Zheludev, I. N.; Hagey, R. J.; Wu, M. T.-P.; Haslecker, R.; Hou, Y. J.; Kretsch, R.; Pintilie, G. D.; Rangan, R.; Kladwang, W.; et al.. Cryo-Electron Microscopy and Exploratory Antisense Targeting of the 28-KDa Frameshift Stimulation Element from the SARS-CoV-2 RNA Genome. *bioRxiv*, **2020**, preprint.

(5) Abraham, M. J.; Murtola, T.; Schulz, R.; Páll, S.; Smith, J. C.; Hess, B.; Lindahl, E. GROMACS: High Performance Molecular Simulations through Multi-Level Parallelism from Laptops to Supercomputers. *SoftwareX* **2015**, *1*−*2*, 19−25.

(6) MacKerell, A. D.; Wiorkiewicz-Kuczera, J.; Karplus, M. An All-Atom Empirical Energy Function for the Simulation of Nucleic Acids. *J. Am. Chem. Soc.* **1995**, *117* (48), 11946.

(7) Atkins, J. F.; Loughran, G.; Bhatt, P. R.; Firth, A. E.; Baranov, P. V. Ribosomal Frameshifting and Transcriptional Slippage: From Genetic Steganography and Cryptography to Adventitious Use. *Nucleic Acids Res.* **2016**, *44* (15), 7007−7078.

(8) Niknamian, S. On the Neglected Shifting Balance Theory, Bateson− Dobzhansky−Muller Model & Quantum Evolution Plus the Role of Mitochondrial Membrane Potential (Mmp) Impact on Covid-19. *Open Access J. Oncol. Med.* **2021**, *4* (3), 384.

(9) Neupane, K.; Munshi, S.; Zhao, M.; Ritchie, D. B.; Ileperuma, S. M.; Woodside, M. T. Anti-Frameshifting Ligand Active against SARS Coronavirus-2 Is Resistant to Natural Mutations of the Frameshift-Stimulatory Pseudoknot. *J. Mol. Biol.* **2020**, *432* (21), 5843−5847.

(10) Park, S.-J.; Kim, Y.-G.; Park, H.-J. Identification of RNA Pseudoknot-Binding Ligand That Inhibits the −1 Ribosomal Frameshifting of SARS-Coronavirus by Structure-Based Virtual Screening. *J. Am. Chem. Soc.* **2011**, *133* (26), 10094−10100.

(11) Mark, P.; Nilsson, L. Structure and Dynamics of the TIP3P, SPC, and SPC/E Water Models at 298 K. *J. Phys. Chem. A* **2001**, *105* (43), 9954−9960.

(12) Darnell, M. E. R.; Subbarao, K.; Feinstone, S. M.; Taylor, D. R. Inactivation of the Coronavirus That Induces Severe Acute Respiratory Syndrome, SARS-CoV. *J. Virol. Methods* **2004**, *121* (1), 85−91.

(13) Hess, B.; Bekker, H.; Berendsen, H. J. C. LINCS: A Linear Constraint Solver for Molecular Simulations. *J. Comput. Chem.* **1997**, *18* (12), 1463.

(14) Bussi, G.; Donadio, D.; Parrinello, M. Canonical Sampling through Velocity Rescaling. *J. Chem. Phys.* **2007**, *126* (1), No. 014101.

(15) Martyna, G. J.; Klein, M. L.; Tuckerman, M. Nosé−Hoover Chains: The Canonical Ensemble via Continuous Dynamics. *J. Chem. Phys.* **1992**, *97* (4), 2635−2643.

(16) Parrinello, M.; Rahman, A. Polymorphic Transitions in Single Crystals: A New Molecular Dynamics Method. *J. Appl. Phys.* **1981**, *52* (12), 7182−7190.

(17) Essmann, U.; Perera, L.; Berkowitz, M. L.; Darden, T.; Lee, H.; Pedersen, L. G. A Smooth Particle Mesh Ewald Method. *J. Chem. Phys.* **1995**, *103* (19), 8577−8593.

(18) Bergonzo, C.; Henriksen, N. M.; Roe, D. R.; Swails, J. M.; Roitberg, A. E.; Cheatham, T. E. Multidimensional Replica Exchange Molecular Dynamics Yields a Converged Ensemble of an RNA Tetranucleotide. *J. Chem. Theory Comput.* **2014**, *10* (1), 492−499.

(19) Price, D. J.; Brooks, C. L. A Modified TIP3P Water Potential for Simulation with Ewald Summation. *J. Chem. Phys.* **2004**, *121* (20), 10096−10103.

(20) Gajdoš, P.; Ježowicz, T.; Uher, V.; Dohnálek, P. A Parallel Fruchterman−Reingold Algorithm Optimized for Fast Visualization of Large Graphs and Swarms of Data. *Swarm Evol. Comput.* **2016**, *26*, 56−63.

(21) Maisuradze, G. G.; Liwo, A.; Scheraga, H. A. Relation between Free Energy Landscapes of Proteins and Dynamics. *J. Chem. Theory Comput.* **2010**, *6* (2), 583−595.

(22) Frugier, M.; Schimmel, P. Subtle Atomic Group Discrimination in the RNA Minor Groove. *Proc. Natl. Acad. Sci. U. S. A.* **1997**, *94* (21), 11291−11294.

(23) El Hassan, M. A.; Calladine, C. R. Two Distinct Modes of Protein-Induced Bending in DNA 1 1Edited by J. Karn. *J. Mol. Biol.* **1998**, *282* (2), 331−343.

(24) Duan, S.-M.; Zhao, X.-S.; Wen, R.-F.; Huang, J.-J.; Pi, G.-H.; Zhang, S.-X.; Han, J.; Bi, S.-L.; Ruan, L.; Dong, X.-P. Stability of SARS Coronavirus in Human Specimens and Environment and Its Sensitivity to Heating and UV Irradiation. *Biomed. Environ. Sci.* **2003**, *16* (3), 246−255.

(25) Lu, R.; Zhao, X.; Li, J.; Niu, P.; Yang, B.; Wu, H.; Wang, W.; Song, H.; Huang, B.; Zhu, N.; et al. Genomic Characterisation and Epidemiology of 2019 Novel Coronavirus: Implications for Virus Origins and Receptor Binding. *Lancet* **2020**, *395* (10224), 565−574.

(26) Haider, S.; Parkinson, G. N.; Neidle, S. Molecular Dynamics and Principal Components Analysis of Human Telomeric Quadruplex Multimers. *Biophys. J.* **2008**, *95* (1), 296−311.

(27) Miner, J. C.; García, A. E. Equilibrium Denaturation and Preferential Interactions of an RNA Tetraloop with Urea. *J. Phys. Chem. B* **2017**, *121* (15), 3734−3746.

(28) Priyakumar, U. D.; Hyeon, C.; Thirumalai, D.; MacKerell, A. D. Urea Destabilizes RNA by Forming Stacking Interactions and Multiple Hydrogen Bonds with Nucleic Acid Bases. *J. Am. Chem. Soc.* **2009**, *131* (49), 17759−17761.

(29) Nikolova, E. N.; Al-Hashimi, H. M. Thermodynamics of RNA Melting, One Base Pair at a Time. *RNA* **2010**, *16* (9), 1687−1691.

(30) Luo, H.; Ye, F.; Sun, T.; Yue, L.; Peng, S.; Chen, J.; Li, G.; Du, Y.; Xie, Y.; Yang, Y.; et al. In Vitro Biochemical and Thermodynamic

Characterization of Nucleocapsid Protein of SARS. *Biophys. Chem.* **2004**, *112* (1), 15−25.
(31) Miner, J. C.; Chen, A. A.; García, A. E. Free-Energy Landscape of a Hyperstable RNA Tetraloop. *Proc. Natl. Acad. Sci. U. S. A.* **2016**, *113* (24), 6665−6670.

https://doi.org/10.1021/acs.jpcb.1c05795
J. Phys. Chem. B 2021, 125, 10672−10681